Journal of Sound and Vibration 329 (2010) 3587–3595

Contents lists available at ScienceDirect

Journal of Sound and Vibration

journal homepage: www.elsevier.com/locate/jsvi

Squeak noise in lead screw systems: Self-excited vibration of continuous model

Jaeyoung Kang, Keysun Kim *

Division of Mechanical and Automotive Engineering, College of Engineering, Kongju National University, Cheonan-Si, Republic of Korea

ARTICLE INFO

Article history:
Received 1 October 2009
Received in revised form
4 March 2010
Accepted 12 March 2010
Handling Editor H. Ouyang
Available online 7 April 2010

ABSTRACT

The dynamic instability of a spinning lead screw in contact with a screw nut is investigated analytically. The lead screw is modeled as a circular beam vibrating in transverse and torsion direction. The contact kinematics between the lead screw and the nut is described on the contact threads in the lead screw. The onset of squeak noise is numerically predicted with a variety of system parameters. Stability analysis shows that the transverse vibration modes can generate squeak noise in the lead screw system. It is highlighted that squeak noise can be controlled by system design parameters in such a manner that the squeak propensity is dependent on rotation speed, screw radius, axial load, contact location, and so on.

1. Introduction

Lead screw system is one of typical mechanical parts in industry. It converts rotating to translating motion by contact forces on the threads in the lead screw and the nut. Friction force during operation may cause the friction-induced vibrations generating squeak noise. For example, noise problem in the lead screw components of the automotive seat system has been often and consistently claimed in the field. Olofsson et al. [1] experimentally investigated the squeak noise of the lead screw system and concluded that the transverse vibration is the squeak mode. Also, they found that the squeak propensity is highly dependent on the location of the nut on the lead screw. Gallina et al. [2] used a 2DOF model for describing the self-excited vibration in the screw-nut system and showed that the moment of inertia is one of the key system parameters in controlling squeak noise. Vahid et al. [3] studied on squeak noise induced by the torsion mode of the rigid lead screw system by using a 4DOF lumped-mass model. Their results showed that rotation speed and axial load influences squeak propensity. These findings in the literature give valuable insight on squeak noise problem in the lead screw-nut system. However, these simplified lumped-mass models have limitation on investigating squeak problems. Nevertheless, the more accurate continuous model has not been developed yet.

The friction-induced noise has been one popular topic in the field of vibration and acoustics that is broadly summarized in [4]. Akay [5] presented the various examples of friction noise and the corresponding analytical or experimental results in his review article. Most of all, the major application exhibiting friction-induced noise problem is disc brake squeal. Many researchers and engineers in academia and industry have investigated for several decades. Broad and valuable information on friction-induced noise mechanisms has been accumulated in this single topic as described in the review articles [6–7]. Some of detailed mechanisms associated with disc brake systems are well described in the series of articles [8–15]. In the brake squeal modeling, the rotation and vibration of the disc are incorporated in the friction-engaged equations of motion

* Corresponding author.
E-mail addresses: jkang@kongju.ac.kr (J. Kang), keysun@kongju.ac.kr (K. Kim).

0022-460X/$ - see front matter © 2010 Elsevier Ltd. All rights reserved.
doi:10.1016/j.jsv.2010.03.018

by describing the contact kinematics of a rotating disc in contact with two stationary pads in the mathematical and numerical manners. The eigensolutions through the linearization about the steady-sliding provide the onset of squeal with respect to system parameters. Mode-coupling [8–9], gyroscopic/negative friction slope destabilization [11,12], moving load effects [14], follower force [15] and modal damping difference [11] are found to be the potential sources of squeal vibrations. Experimental investigation [16] has been also conducted to validate the mode lock-in mechanism in relation to brake squeal. It must be noted that these findings are not limited to the disc brake squeal, but extended to the general friction-induced noise.

In this paper, the modeling methodology of a disc brake model is applied to the other practical problem: lead screw squeak. The contact forces are defined on the thread of the rotating lead screw in contact with a nut. The Coulomb's friction law with a nonlinear friction-velocity curve is applied on the frictional contact model. From the assumed modes method and the linearization process, the linear equations of motion of the screw squeak model are derived. The eigensensitivity analysis associated with several design parameters are conducted in order to provide system design perspective for squeak reduction in the lead screw system.

2. Derivation of equations of motion

The lead screw system is composed of a uniform spinning circular beam in contact with a nut as shown in Fig. 1. The lead screw has an effective radius (R) and a screw helix angle of a square thread (β). It is subject to the hinged boundary condition at the both ends in the transverse direction. Also, the torsional motion of the lead screw is assumed to be clamped at the one end and free at the other end. This may correspond to a motor drive and free bearing in the motor drive system. The mating part of the lead screw is a nut with a length (b) and its location is denoted by (z_o). The spinning speed (Ω) generates contact forces on the contact between the threads of the screw and nut, resulting in the axial motion of the lead screw as shown in Fig. 2. The normal stress (N_o) on the contact thread between the lead screw and nut is assumed to be uniform over the contact. It is assumed that the nut is floating in the transverse direction and nut material is much softer than the lead screw material so that the clamping effect of the nut is neglected in this analysis.

The shearing effects are neglected so that the Bernoulli–Euler beam theory is applied in the analysis [17]. Therefore, the displacement vector of a position B is described in the reference frame (X,Y,Z) such that:

$$\mathbf{r}_B = \mathbf{r}_A + \mathbf{r}_{B/A}, \tag{1}$$

$$\mathbf{r}_{B/A} = r\mathbf{e}_r + z\mathbf{k} + u\mathbf{i} + v\mathbf{j} + r\xi\mathbf{e}_\theta, \tag{2}$$

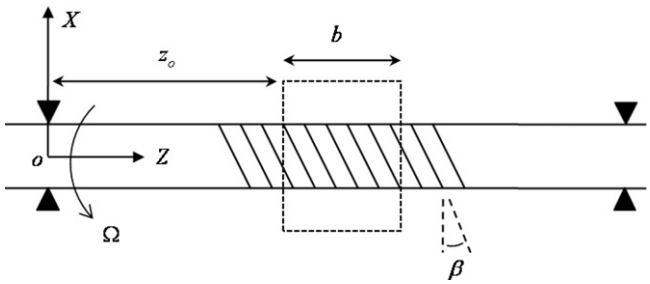

Fig. 1. Configuration of lead screw system.

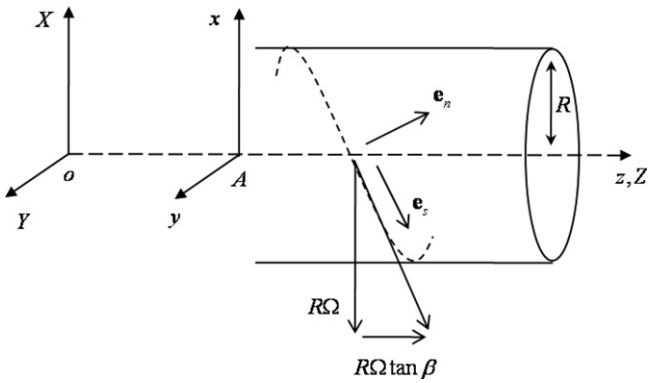

Fig. 2. Translation in the axial direction.

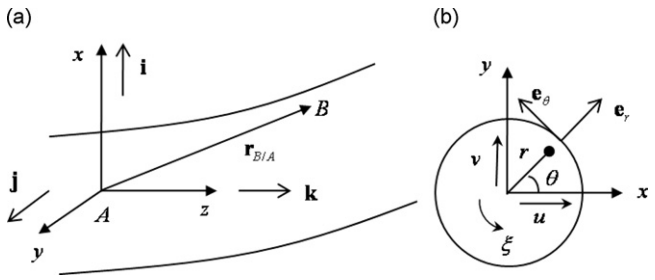

Fig. 3. Position and displacement vectors: (a) relative position; (b) components of displacement.

where $\mathbf{r}_A$ represents the displacement of the undeformed centre of the lead screw in the axial direction and where u and v are the transverse deflection in x and y directions, and ξ is the torsional deflection (Fig. 3). The velocity vector of a position B is the derivative of Eq. (1) in time:

$$\mathbf{V}_B = \mathbf{V}_A + (\dot{\mathbf{r}}_{B/A})_{xyz} + \boldsymbol{\omega} \times \mathbf{r}_{B/A}, \tag{3}$$

where

$$\mathbf{V}_A = R\Omega \tan\beta \mathbf{k}, \tag{4}$$

$$\boldsymbol{\omega} = \Omega \mathbf{k}. \tag{5}$$

The axial load F_z is assumed to be known so that the normal stress on the thread N_o is derived from:

$$F_z = \int_{A_c} \{\langle \mathbf{N}_o, -\mathbf{k}\rangle + \langle \mu N_o \mathbf{e}_s, -\mathbf{k}\rangle\} \mathrm{d}A, \tag{6}$$

where A_c stands for the contact area, $\langle \cdot, \cdot \rangle$ is the inner product between two vectors and

$$\mathbf{N}_o = -N_o \mathbf{e}_n, \tag{7}$$

$$\mathbf{e}_n = -\sin\beta \mathbf{e}_\theta + \cos\beta \mathbf{k}. \tag{8}$$

By the assumption of uniform contact over the square thread with the height h, Eq. (6) reduces to:

$$N_o = \frac{F_z}{hR\alpha(1+\mu\tan\beta)}, \tag{9}$$

where α is total angle in radians of the thread in contact with the nut.

The friction force per unit area on the thread of the lead screw is obtained from Coulomb's law of friction as:

$$\mathbf{f} = -\mu \cdot N_o \cdot \frac{\mathbf{V}_c}{|\mathbf{V}_c|}, \tag{10}$$

where the sliding velocity at the contact $\mathbf{V}_c$ is the velocity when the position B is located at the contact region such that:

$$\mathbf{V}_c = \mathbf{V}_B(r = R, z_o \le z \le z_o + b). \tag{11}$$

Here, the friction curve with the negative friction slope [11–12] is applied in the analysis as:

$$\mu = \mu_k + (\mu_s - \mu_k) \cdot \exp(-d|\mathbf{V}_c|), \tag{12}$$

where μ_s, μ_k and d are the control parameters determining the magnitude and the slope of the friction coefficient. The corresponding virtual work by contact forces is obtained from:

$$\delta W_c = \int_{A_c} \langle \mathbf{f} + \mathbf{N}_o, \delta \mathbf{u}_c \rangle \, \mathrm{d}A, \tag{13}$$

where $\mathbf{u}_c$ is the deflection vector at a contact location given by:

$$\mathbf{u}_c = u\mathbf{i} + v\mathbf{j} + R\xi \mathbf{e}_\theta. \tag{14}$$

The potential energy and the homogeneous part of the kinetic energy and of the lead screw are described as:

$$U = \frac{1}{2} EI_{xx} \int_0^L u''^2 \, \mathrm{d}z + \frac{1}{2} EI_{yy} \int_0^L v''^2 \, \mathrm{d}z + \frac{1}{2} GI_{zz} \int_0^L \xi''^2 \, \mathrm{d}z, \tag{15}$$

and

$$T = \int_0^L \int_0^{2\pi} \int_0^R (dT) r \, \mathrm{d}r \, \mathrm{d}\theta \, \mathrm{d}z, \tag{16}$$

where EI_{xx}, EI_{yy}, GI_{zz} are the bending and torsion rigidity in YZ, XZ and XY planes, respectively, and where

$$dT = \frac{\rho}{2}\left\{(\dot{u}-\Omega v - r\Omega\xi\cos\theta - r\dot{\xi}\sin\theta)^2 + (\dot{v}+\Omega u - r\Omega\xi\sin\theta + r\dot{\xi}\cos\theta)^2\right\}. \tag{17}$$

By using the assumed modes method [8–13], the discretized equations of motion for the lead screw subject to friction on the thread are derived as:

$$\frac{\mathrm{d}}{\mathrm{d}t}\left[\frac{\partial(T-U)}{\partial\dot{q}_m}\right] - \frac{\partial(T-U)}{\partial q_m} = \sum_{n=1}^{N} Q_{mn}(q_n), \quad m = 1,\ldots,N, \tag{18}$$

where N is the number of the truncated modes of the lead screw including the transverse and torsion modes and where the modal coordinates and forces are:

$$\mathbf{q} = \{q_1 \;\; q_2 \;\; \cdots \;\; q_N\}, \tag{19}$$

$$\delta W_c \equiv \sum_{m=1}^{N}\sum_{n=1}^{N} Q_{mn}(q_n)\cdot\delta q_m. \tag{20}$$

Here Q_{mn} is the generalized force that produces the system matrices, (A.3)–(A.8) of Appendix A by the linear process.

The trial functions used in the above assumed modes model are the eigenmodes of the bending and torsion vibration of the uniform beam subject to the given boundary conditions:

$$u(z,t) \cong \sum_{n=1}^{N} \Phi_n^x(z)\cdot q_n(t), \tag{21}$$

$$v(z,t) \cong \sum_{n=1}^{N} \Phi_n^y(z)\cdot q_n(t), \tag{22}$$

$$\xi(z,t) \cong \sum_{n=1}^{N} \Phi_n^\theta(z)\cdot q_n(t), \tag{23}$$

where the mass-normalized mode shape functions are:

$$\Phi_n^x(z) = \frac{1}{\sqrt{3}R}\sqrt{\frac{2}{\rho\pi L}}\sin\left(\frac{n\pi z}{L}\right) \text{ for transverse mode in } x\text{-direction, otherwise, } 0, \tag{24}$$

$$\Phi_n^y(z) = \frac{1}{\sqrt{3}R}\sqrt{\frac{2}{\rho\pi L}}\sin\left(\frac{n\pi z}{L}\right) \text{ for transverse mode in } y\text{-direction, otherwise, } 0, \tag{25}$$

$$\Phi_n^\theta(z) = \frac{1}{\sqrt{3}R}\sqrt{\frac{2}{\rho\pi L}}\sin\left(\frac{(2n-1)\pi z}{2L}\right) \text{ for torsion mode, otherwise, } 0, \tag{26}$$

It should be noted that z in the mode shape functions of Eqs. (24)–(26) is equivalent to $(R\tan\beta)\theta$ for the integration of the mode shape function over the contact in Eq. (13) and Eqs. (A.3)–(A.8) of Appendix A.

By linearizing the nonlinear equations of motion (18) at the steady-sliding state and including the modal damping intrinsic to the system, the linearized equations take the form:

$$\ddot{\mathbf{q}} + (\mathbf{C}+\mathbf{G}+\mathbf{W}_3+\mathbf{W}_4+\mathbf{W}_{5\dot{q}})\dot{\mathbf{q}} + ([\omega^2]-\Omega^2\mathbf{I}+\mathbf{W}_1+\mathbf{W}_2+\mathbf{W}_{5q})\mathbf{q} = \mathbf{0}, \tag{27}$$

where $[\omega]^2$ is the natural frequency matrix of the lead screw component and the other system matrices are described in Appendix A. Substituting $\mathbf{q}(t) = \mathbf{A}e^{\lambda t}$ into Eq. (27) and solving $\mathrm{Re}(\lambda)$ and $\mathrm{Im}(\lambda)$ of the characteristic equation will determine the onset of dynamic instability for $\mathrm{Re}(\lambda) > 0$ and $\mathrm{Im}(\lambda) \neq 0$, where λ is the eigenvalues of the friction-engaged system.

3. Numerical results

The modal analysis and stability results will be obtained from the prescribed boundary conditions, dimensions and the material properties of the lead screw system for an automotive seat system as summarized in Table 1. The natural frequencies and the corresponding mode shapes are described in Table 2, where each of bending modes is the pair mode in the transverse direction. Eighteen eigenmodes (N=18) including 12 bending and 6 torsion modes are found to provide convergent stability results and used for the subsequent analysis. The velocity-dependent friction coefficient is selected from the data presented in [3], where the control parameters of friction coefficient are $(\mu_s,\mu_k,d) = (0.25,0.2,10)$ (Fig. 4).

For a preliminary stability analysis, the real and imaginary parts of the eigenvalues of the system modes are traced with the variation of rotation speed. The stability analysis is restricted to the subcritical speed throughout the paper. Fig. 5 illustrates that the real part of each mode varies with respect to rotation speed. Some of real part loci exist in the region of

Table 1
Nominal values of system parameters.

Parameter	Symbol	Value
Effective radius	R	5 mm
Length of lead	L	300 mm
Height of thread	h	1 mm
Screw helix angle	β	5°
Contact location	z_o	150 mm
Contact length	b	60 mm
Young's modulus	E	207 GPa
Shear modulus	G	79.3 GPa
Density	ρ	7820 kg m^{-3}
Axial load	F_z	200 N
Modal damping coefficient	ξ_n	3.0×10^{-3}

Table 2
Natural frequencies of the uncoupled lead screw.

n	1,2	3,4	5,6	7	8,9	10,11	12	13,14
(Hz)	224	898	2020	2654	3592	5612	7961	8082
Mode	1st B	2nd B	3rd B	1st T	4th B	5th B	2nd T	6th B

B: bending mode, T: torsion mode.

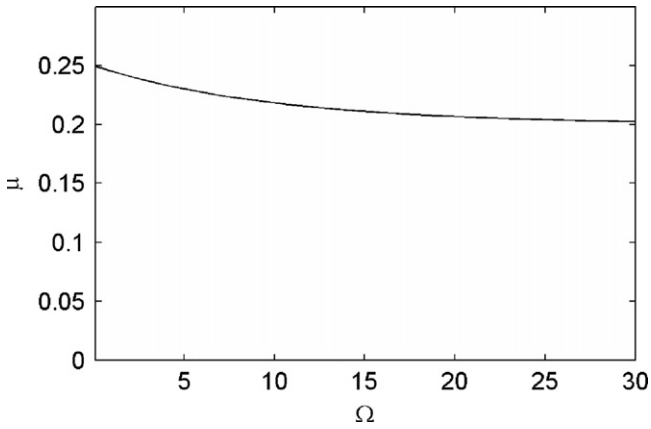

Fig. 4. Friction–velocity curve.

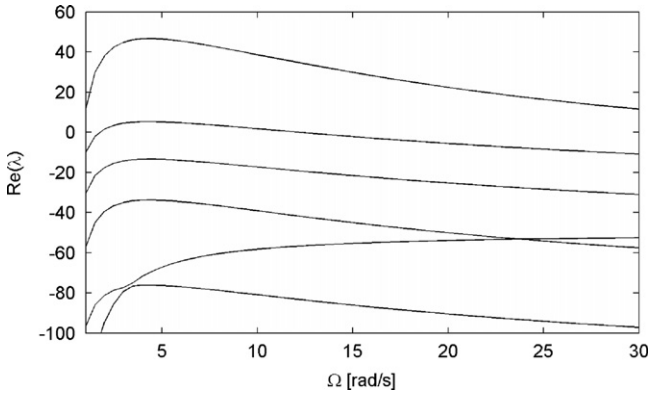

Fig. 5. Squeak propensity with respect to rotation speed.

$\mathrm{Re}(\lambda) > 0$, where these modes will be referred to as the squeak modes. It is seen that the real parts of eigenvalues are highly dependent on the sliding speed, where some of real parts increase with the decrease of rotation speed, but the others do not. Near the zero speed, all real parts drop. These rotation effects are strongly attributed to the negative slope of the velocity dependent friction coefficient and the radial slip perpendicular to the rotation direction. It is well described in [11–13] in the application of a disc brake squeal. It should be noted that the radial dissipative effect in the linearized equations of motion (27) comes from the linearization of Eq. (10). As Ω goes to zero, the linear term of the linearized friction force in Eq. (10) vanishes and system variables become nonlinear. Therefore, the nonlinear analysis should be adopted for investigating the dynamic behavior on the verge of zero rotation speed. It may be referred to the article [10] presenting the nonlinear behavior in brake squeal.

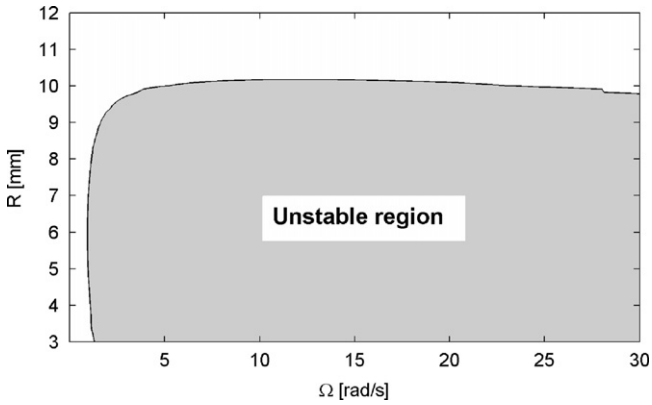

Fig. 6. Stability boundary with respect to rotation speed and effective radius.

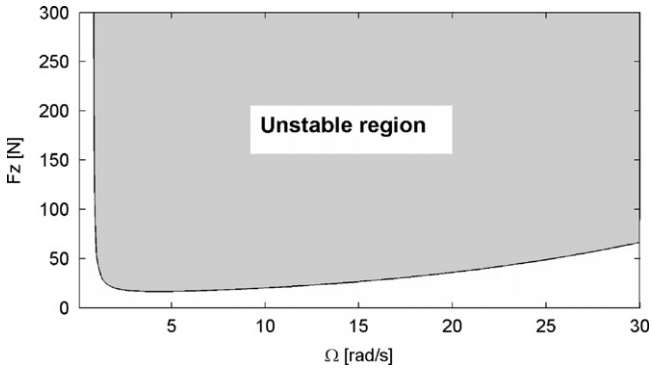

Fig. 7. Stability boundary with respect to rotation speed and axial load.

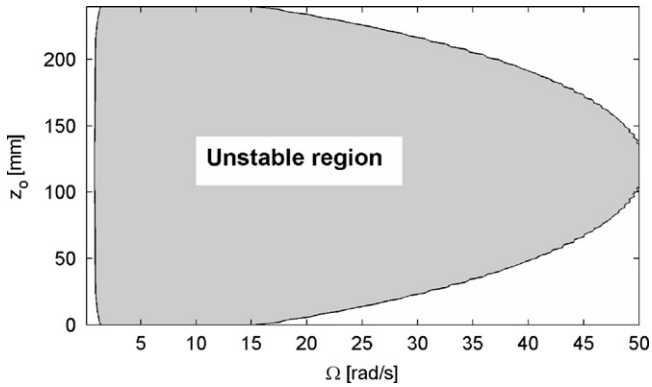

Fig. 8. Stability boundary with respect to rotation speed and contact location.

For the parametric stability analysis, several system parameters are used in the eigenvalue sensitivity analysis. The effective radius, axial load and contact locations are chosen for the parameters of the following sensitivity analysis associated with rotation speed variation. Fig. 6 demonstrates that the increase of the effective radius can stabilize the system over the broad rotation speed range in the manner that there is an upper bound of the dynamic instability over the rotation speeds. Also, it is found that there is an lower bound of the axial load for the unstable regime as in Fig. 7. The increase of the axial load destabilizes the system, particularly in the low speed region. Similarly, the dynamic instability is shown to be sensitive to the contact location (or the location of screw nut) and its propensity reaches maximum over the broad speed range when the screw nut is located at the center of the lead screw as illustrated in Fig. 8. It is noted that the stabilization at the very low speed in Fig. 6–8 is due to the radial slip dissipation as explained in relation to Fig. 5.

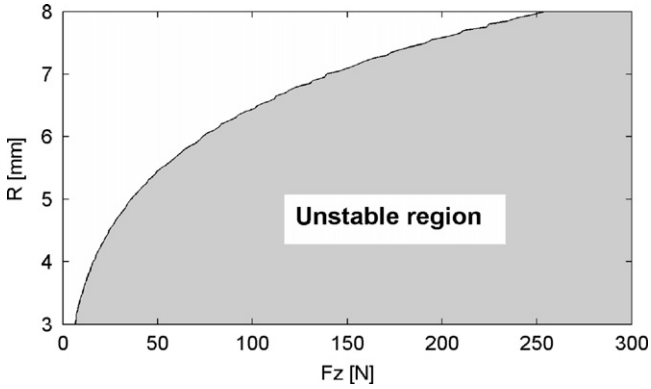

Fig. 9. Stability boundary with respect to axial load and effective radius at $\Omega = 20\,\mathrm{rad/s}$].

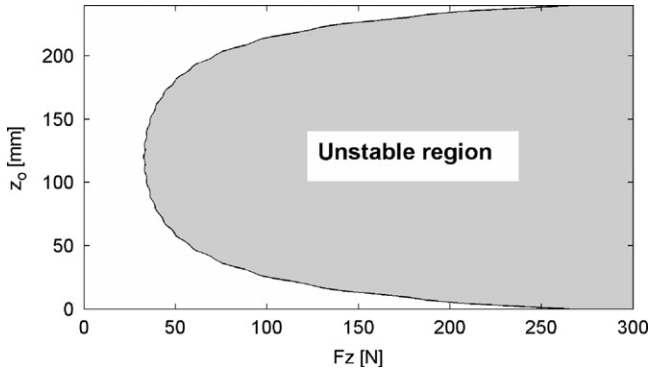

Fig. 10. Stability boundary with respect to axial load and contact location at $\Omega = 20\,\mathrm{rad/s}$.

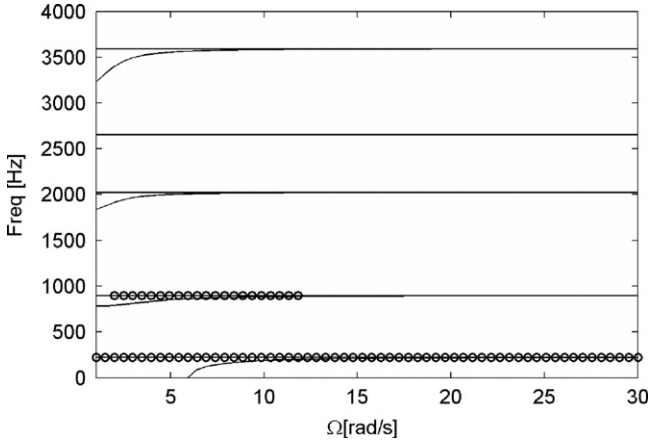

Fig. 11. Squeak frequencies with respect to rotation speed, thick line: $\mathrm{Re}(\lambda) > 0$.

In some mechanical applications such as a powered automotive seat adjuster, the rotation speed is a fixed value during operation. For a given rotation speed, the stability boundary is determined through the eigenvalue sensitivity analysis as the following. Fig. 9 shows that the decrease of the effective radius and the increase of the axial load can contribute to the system destabilization for a given rotation speed. Besides, Fig. 10 demonstrates that the change of contact location can influence the squeak propensity as described in Fig. 8.

In order to determine the squeak modes, the unstable frequencies with the positive real parts are identified on the speed–frequency plot as demonstrated in Fig. 11. The mode shapes corresponding to the squeak frequencies are the first and second bending modes of the lead screw. Therefore, it is important to note that the squeak noise of the lead screw system can be induced by the bending vibration modes.

4. Conclusions and discussion

The mathematical screw squeak model has been constructed through the 3D contact kinematics and the assumed mode method. The friction force vector is defined by the relative velocity vector on the contact thread between the rotating and translating lead screw and the nut located at a given axial position of the lead screw. The linearized friction-coupled equations of motion provide the stability boundaries with respect to system design parameters.

In the stability analysis, squeak propensity is found to be highly dependent on the sliding speed. The lead screw system is prone to be stable at high and very low speeds, but unstable at moderate speeds. This is due to the dependency of negative friction–velocity slope to the sliding speed and the radial slip dissipation. Most of all, the negative friction–velocity slope takes an essential role on generating squeak noise in the analysis. It is shown that squeak propensity can be effectively controlled by system design parameters such as axial load, screw radius and contact location.

For the given system parameters in Table 1, the first and second bending modes are seen to be squeak modes at a certain range of rotation speed. The ensuing parametric stability results, therefore, are related to the sensitivity of the stability to these transverse vibration modes. It implies that the stability analysis for the purpose of squeak reduction design should be performed on the basis of modal stability criterion with respect to system design parameters.

Acknowledgment

This work was partly supported by Advanced Motor Parts Regional Innovation Center (AMP.RIC) of Kongju National University administered by MKE (Ministry of Knowledge Economy), Korea. The authors are grateful to Prof. Chuck Krousgrill (Purdue University) for valuable comments and discussions on a revision of this paper.

Appendix A. The matrices of the linearized equations of motion

$$\mathbf{C} = 2\xi_n \cdot \mathbf{diag}(\omega_n), \tag{A.1}$$

$$\mathbf{G} = 2\rho\Omega \int_0^L \int_0^{2\pi} \int_0^R (-[\Phi_i^x \Phi_j^y] + [\Phi_i^y \Phi_j^x]) r \, \mathrm{d}r \, \mathrm{d}\theta \, \mathrm{d}z, \tag{A.2}$$

$$\mathbf{W}_1 = \frac{\mu_o F_z}{\alpha R} \int_{\alpha_o}^{\alpha_o+\alpha} \Big\{ \sin\theta\cos\theta\cos^2\beta[\Phi_i^x\Phi_j^x] - (\cos^2\theta + \sin^2\theta\sin^2\beta)[\Phi_i^x\Phi_j^y] + (\sin^2\theta + \cos^2\sin^2\beta)[\Phi_i^y\Phi_j^x] - \sin\theta\cos\theta\cos^2\beta[\Phi_i^y\Phi_j^y] \Big\} \, \mathrm{d}\theta, \tag{A.3}$$

$$\mathbf{W}_2 = \frac{\mu_o F_z}{\alpha} \int_{\alpha_o}^{\alpha_o+\alpha} \Big\{ -\cos\theta[\Phi_i^x\Phi_j^\theta] - \sin\theta[\Phi_i^y\Phi_j^\theta] + \cos\theta\sin^2\beta[\Phi_i^\theta\Phi_j^x] + \sin\theta\sin^2\beta[\Phi_i^\theta\Phi_j^y] \Big\} \mathrm{d}\theta, \tag{A.4}$$

$$\mathbf{W}_3 = \frac{\mu_o F_z}{R\Omega\alpha} \int_{\alpha_o}^{\alpha_o+\alpha} \Big\{ (\cos^2\theta + \sin^2\theta\sin^2\beta)[\Phi_i^x\Phi_j^x] - \sin\theta\cos\theta\cos^2\beta[\Phi_i^x\Phi_j^y] - \sin\theta\cos\theta\sin^2\beta[\Phi_i^y\Phi_j^x] + \cos^2\theta\sin^2\beta[\Phi_i^y\Phi_j^y] + \sin^2\beta[\Phi_i^\theta\Phi_j^\theta] \Big\} \mathrm{d}\theta, \tag{A.5}$$

$$\mathbf{W}_4 = \frac{\mu_o F_z \sin^2\beta}{\Omega\alpha} \int_{\alpha_o}^{\alpha_o+\alpha} \Big\{ -\sin\theta[\Phi_i^x\Phi_j^\theta] + \cos\theta[\Phi_i^y\Phi_j^\theta] - \sin\theta[\Phi_i^\theta\Phi_j^x] + \cos\theta[\Phi_i^\theta\Phi_j^y] \Big\} \mathrm{d}\theta, \tag{A.6}$$

$$\mathbf{W}_{5q} = \frac{F_z\Omega\gamma}{\alpha}(1-\tan^2\beta) \int_{\alpha_o}^{\alpha_o+\alpha} \Big\{ -\sin\theta\cos\theta[\Phi_i^x\Phi_j^x] + \cos\theta\sin\theta[\Phi_i^y\Phi_j^y] - \sin^2\theta[\Phi_i^x\Phi_j^y] + \cos^2\theta[\Phi_i^y\Phi_j^x] + R\cos\theta[\Phi_i^\theta\Phi_j^x] + R\sin\theta[\Phi_i^\theta\Phi_j^y] \Big\} \mathrm{d}\theta, \tag{A.7}$$

$$\mathbf{W}_{5\dot{q}} = \frac{F_z\gamma}{\alpha}(1-\tan^2\beta) \int_{\alpha_o}^{\alpha_o+\alpha} \Big\{ -\sin^2\theta[\Phi_i^x\Phi_j^x] + \cos^2\theta[\Phi_i^y\Phi_j^y] - \cos\theta\sin\theta[\Phi_i^x\Phi_j^y] + \cos\theta\sin\theta[\Phi_i^y\Phi_j^x] + R\sin\theta[\Phi_i^\theta\Phi_j^x]$$

$$+R\cos\theta[\Phi_i^{\theta}\Phi_j^{y}]-R\sin\theta[\Phi_i^{x}\Phi_j^{\theta}]+R\cos\theta[\Phi_i^{y}\Phi_j^{\theta}]+R^2[\Phi_i^{\theta}\Phi_j^{\theta}]\Big\}\mathrm{d}\theta, \tag{A.8}$$

where

$$\alpha_o = z_o/(R\tan\beta), \tag{A.9}$$

$$\mu_o = \mu|_{\mathbf{v}_c=0}, \tag{A.10}$$

$$\gamma = -(\mu_s-\mu_k)d\exp(-dR\Omega/\cos\beta)\cos\beta. \tag{A.11}$$

References

[1] U. Olofsson, L. Ekerfors, Friction-induced noise in screw-nut transmissions, *Wear* 148 (1991) 25–37.
[2] P. Gallina, Vibration in screw jack mechanisms: experimental results, *Journal of Sound and Vibration* 282 (2005) 1025–1041.
[3] O. Vahid, N. Eslaminasab, Friction-induced vibration in lead screw systems: mathematical modeling and experimental studies, *Journal of Vibration and Acoustics* 131 (2009) 021003 (10pages).
[4] G. Sheng, *Friction-induced Vibrations and Sound; Principles and Applications*, CRC Press, Boca Raton, 2008.
[5] A. Akay, Acoustics of friction, *Journal of Acoustical Society of America* 111 (2002) 1525–1548.
[6] N.M. Kinkaid, O.M. O'Reilly, P. Papadopoulos, Automotive disc brake squeal, *Journal of Sound and Vibration* 267 (2003) 105–166.
[7] H. Ouyang, W. Nack, Y. Yuan, F. Chen, Numerical analysis of automotive disc brake squeal: a review, *International Journal of Vehicle Noise and Vibration* 1 (2005) 207–231.
[8] J. Kang, C.M. Krousgrill, F. Sadeghi, Dynamic instability of a thin plate with friction interface and its application to disc brake squeal, *Journal of Sound and Vibration* 316 (2008) 164–179.
[9] J. Kang, C.M. Krousgrill, F. Sadeghi, Analytical formulation of mode-coupling instability in disc-pad coupled system, *International Journal of Mechanical Science* 51 (2009) 52–63.
[10] J. Kang, C.M. Krousgrill, F. Sadeghi, Wave pattern motion and stick-slip limit cycle oscillation of a squealing disc, *Journal of Sound and Vibration* 325 (2009) 552–564.
[11] J. Kang, C.M. Krousgrill, F. Sadeghi, Comprehensive stability analysis of disc brake vibrations including gyroscopic, negative friction slope and mode-coupling mechanisms, *Journal of Sound and Vibration* 324 (2009) 387–407.
[12] J. Kang, Squeal analysis of gyroscopic disc brake system based on finite element method, *International Journal of Mechanical Science* 51 (2009) 284–294.
[13] D. Hochlenert, G.S. Korspeter, P. Hagedorn, Friction induced vibrations in moving continua and their application to brake squeal, *Journal of Applied Mechanics* 74 (2007) 542–549.
[14] H. Ouyang, Q. Cao, J.E. Mottershead, T. Treyde, Vibration and squeal of a disc brake: modeling and experimental results, *Proceedings of Institution of Mechanical Engineers, Part D, Journal of Automobile Engineering* 217 (2003) 867–875.
[15] M.R. North, Disc brake squeal, in: *Braking of Road Vehicles, Automobile Division of the Institution of Mechanical Engineers*, Mechanical Engineering Publications Limited, London, England, 1976 pp. 169–176.
[16] A. Akay, O. Giannini, F. Massi, A. Sestieri, Disc brake squeal characterization through simplified test rigs, *Mechanical Systems and Signal Processing* 23 (2009) 2590–2607.
[17] J.R. Banerjee, H. Su, Development of a dynamic stiffness matrix for free vibration analysis of spinning beams, *Computers and Structures* 82 (2004) 2189–2197.